Bull. Chem. Soc. Ethiop. **2027**, 41(1), 133-147.
DOI: https://dx.doi.org/10.4314/bcse.v41i1.10

ISSN 1011-3924
Printed in Ethiopia
Online ISSN 1726-801X
© 2027 Chemical Society of Ethiopia and The Authors

# CHARACTERIZATION OF GREEN-SYNTHESIZED REDUCED GRAPHENE OXIDE NANOSHEETS FOR STRUCTURAL, MORPHOLOGICAL, AND BIOLOGICAL PROPERTIES

Manal A. Awad[1*], Khalid M. O. Ortashi[2*], H. Alrsheed[3], Wadha Alenazi[4], Eram Eltahir[5], Fatemah M. Barakat[4*]

[1]King Abdullah Institute for Nanotechnology, King Saud University, Riyadh 11451, Saudi Arabia
[2]Department of Chemical Engineering, King Saud University, Riyadh, 11421, Saudi Arabia
[3]Department of Zoology, College of Science, King Saud University, Riyadh, Saudi Arabia
[4]Department of Physics, College of Science, King Saud University, P.O. Box 22452, Riyadh 11459, Saudi Arabia
[5]Department of Pharmaceutics, College of Pharmacy, King Saud University, Riyadh, Saudi Arabia

(Received January 28, 2026; Revised September 22, 2026; Accepted October 13, 2026)

**ABSTRACT**. Two-dimensional graphene derivatives exhibit excellent biocompatibility, structural robustness, and chemical stability, making them promising candidates for biomedical applications. This study presents a sustainable, phytochemical-assisted green approach for the synthesis of reduced graphene oxide (rGO) using Nigella sativa seed (NSS) extract as a natural reducing and stabilizing agent. Comprehensive characterization using XRD, FTIR, TEM, SEM, EDS, XPS, and DLS confirmed the successful reduction of graphene oxide. XRD analysis revealed a broad diffraction peak at $2\theta \approx 25°$, corresponding to the (002) plane of graphitic carbon, while FTIR spectra showed substantial removal of oxygen-containing functional groups with residual biomolecular signatures originating from NSS extract. Electron microscopy demonstrated transparent, crumpled, and wrinkled nanosheets, and EDS analysis confirmed high carbon purity (98.85%). XPS further validated effective deoxygenation and restoration of $sp^2$-hybridized carbon networks. DLS measurements indicated a multimodal size distribution with moderate colloidal stability ($\zeta = +17 \pm 6.58$ mV). Biologically, the NSS- rGO exhibited strong antibacterial activity against Bacillus subtilis, Escherichia coli, and Candida albicans. Additionally, MTT assays revealed dose-dependent anticancer activity against MCF-7 and HCT-116 cell lines, with $IC_{50}$ values of 3.125 and 1.56 mg/mL, respectively. These results highlight the potential of NSS-rGO as a sustainable and effective material for biomedical applications.

**KEY WORDS**: rGO, Nanosheets, Phytochemical synthesis, NSS, Antibacterial, Anticancer

## INTRODUCTION

Graphene is the fundamental basis of other materials such as graphite and carbon nanotubes [1]. Graphene oxide and reduced graphene oxide are examples of functional graphene derivatives, which are regarded as multifunctional, solution-processable next-generation materials. Because of their distinct electrical, optical, mechanical, and chemical characteristics, they are utilized in numerous industries such as energy conversion, electronics, storage technologies, electrochemical sensors, and ultrathin optoelectronics [2,3]. Furthermore, these derivatives, in particular reduced graphene oxide, are being thoroughly investigated for potential application as antibacterial and anticancer delivery systems [4-6]. Recently, many pharmacological studies focused on creating better drug delivery systems that can deliver medications precisely to predetermined sites throughout the body at regulated rates with few adverse effects [7]. In this regard, graphene nanomaterials are receiving much attention, particularly because of their growing capacity to precisely and effectively target cancer cells. Since graphene derivatives have oxygen atoms and

*Corresponding author. E-mail: ortashi9@ksu.edu.sa, mawad@ksu.edu.sa, fbarakat@ksu.edu.sa
This work is licensed under the Creative Commons Attribution 4.0 International License

other functional groups, they offer a great surface on which drug molecules may adhere, making them effective drug carriers [8]. Furthermore, they can be mixed with other biocompatible substances to form hybrid complexes that have desired properties for use in biomedical applications. For example, nano-graphene coated with biocompatible polyethylene glycol (PEG) has been successfully utilized for photothermal ablation of tumors in a mouse model and has shown significant passive tumor absorption *in vivo* [9,10]. Additionally, graphene-based biosensors that use distinct methods to detect different biomolecules have been produced. Even though it is still in its early stages, graphene-based nanomedicine is promising and may soon offer new methods for diagnosing and treating illnesses [11-13]. Recent studies have focused on enhancing the manufacturing of graphene nanoparticles and expanding their surface modification methods to fully realize their potential. In this context, "green" synthesis methods have gained attention, as traditional chemical methods are costly and involve hazardous chemicals and organic solvents [14].

The present study explores the use of NSS extract as a green, scalable, and cost-effective reducing agent for the synthesis of rGO nanosheets. The synthesis methodology has previously been protected by a patent from the same authors and research group [15]. The current work extends this patented technology through comprehensive characterization and biological evaluation of the synthesized rGO nanosheets, providing detailed insights into their structural, optical, surface, and biomedical properties.

## MATERIALS AND METHODS

### *Preparation of seed extract*

The seeds of Nigella sativa were thoroughly washed several times with distilled water to remove dust and surface impurities. Subsequently, 30 g of finely powdered seeds were boiled in 150 mL of double-distilled water for 5 min to facilitate the extraction of bioactive phytochemicals and reducing agents responsible for the reduction and stabilization processes during nanoparticle synthesis. The obtained mixture was centrifuged and filtered, and the filtrate was collected and stored at 4 °C for further use [16].

### *Green synthesis of rGO nanosheets*

Soot generated during the combustion of natural wood during the baking process was collected and utilized as the carbon precursor for graphene oxide (GO) synthesis. The collected soot was purified by washing with dilute HCl (5%) to remove inorganic contaminants and metallic impurities, followed by repeated rinsing with deionized (DI) water until a neutral pH was achieved. The purified soot was then dried at 80 °C prior to further use. Subsequently, the modified Hummers' method was employed due to its effectiveness in oxidizing carbonaceous materials and producing graphene oxide sheets enriched with oxygen-containing functional groups. The modified Hummers' method was employed due to its effectiveness in producing oxygenated graphene oxide sheets from carbonaceous materials. In a typical synthesis, 1 g of soot was dispersed in 50 mL of concentrated $H_2SO_4$ and stirred for 5 min to ensure uniform dispersion and acid activation of the carbon material. Subsequently, 5 g of $KMnO_4$ was gradually added under ice-bath conditions to control the exothermic oxidation reaction and prevent overheating. The suspension was then stirred at 35 °C for 10 min to promote the controlled oxidation of carbon layers, followed by increasing the temperature to 60 °C for 15 min to enhance exfoliation and oxidation efficiency. Continuous addition of NSS extract was performed until the total suspension volume reached 150 mL. The NSS extract served as a natural reducing and stabilizing agent for the conversion of GO into rGO, while the selected temperature facilitated the reduction process without excessive structural damage to the graphene sheets. After 5 min, 5 mL of $H_2O_2$ was added

to terminate the oxidation reaction and reduce residual permanganate and manganese intermediates. The obtained product was subjected to ultrasonic probe treatment to improve exfoliation and dispersion of the nanosheets. The suspension was then centrifuged and repeatedly washed with 5% HCl solution and deionized water to remove residual metal ions, acids, and impurities. Finally, the purified product was dried at 350 °C to obtain rGO nanosheets with improved crystallinity and reduced oxygen-containing functional groups (Figure 1).

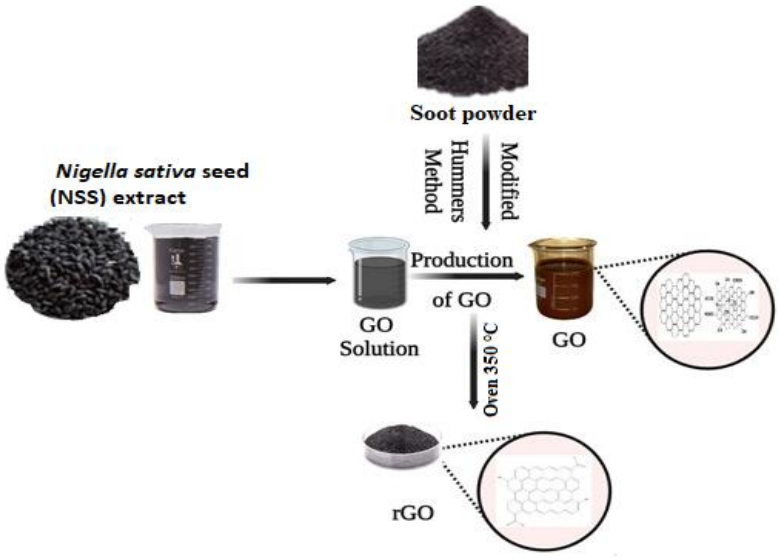



Figure 1. Illustration of the steps of the eco-friendly synthesis of rGO

*Characterization of synthesized rGO nanosheets*

Transmission electron microscopy (JEM-1011; JEOL; Japan) and an X-ray diffractometer (XRD; D8 ADVANCE; Bruker; UK) were used to characterize the product. The structure and morphology of the rGO produced were characterized using scanning electron microscopy (SEM; JEOL-FE SEM), and the presence of elements was verified using energy-dispersive spectroscopy (EDX). The surface functional groups of the as-prepared rGO were characterized using Fourier-transform infrared spectroscopy (FTIR, Shimadzu IR, Prestige 21, Nakagyo-Ku, Kyoto, Japan), with spectra acquired over a range of 4000-500 $cm^{-1}$. The average particle size and zeta potential ($\zeta$) of the synthesized rGO were measured using a Zetasizer (Nano series, HT Laser, ZEN3600, Malvern Instruments, UK) through Dynamic Light Scattering (DLS), providing characterization of the green-synthesized rGO. The surface chemical composition, specifically the presence of carbon and oxygen, was analyzed using X-ray Photoelectron Spectroscopy (XPS) with a JEOL JPS 9030 photoelectron spectrometer equipped with a 500 W X-ray source (JEOL Ltd., Akishima, Tokyo, Japan).

*Screening of antimicrobial activities*

For the antimicrobial assay, pure cultures of fungi including *Aspergillus fumigatus* (RCMB 02567) and *Candida albicans* (RCMB 05038), Gram-positive bacteria such as *Streptococcus pneumoniae* (RCMB 010011) and *Bacillus subtilis* (RCMB 010068), and Gram-negative bacteria including *Pseudomonas aeruginosa* (RCMB 010045), and *Escherichia coli* (RCMB 010054) were employed. The antimicrobial activity of the synthesized rGO nanosheets was evaluated

against selected Gram-positive bacteria, Gram-negative bacteria, and fungal strains using the agar well diffusion method. Fresh microbial cultures were adjusted to approximately $1 \times 10^8$ CFU/mL (0.5 McFarland standard) and uniformly spread onto the surface of sterile Mueller–Hinton agar plates for bacterial strains and Sabouraud dextrose agar plates for fungal strains. The synthesized rGO nanosheets were dispersed in sterile deionized water and sonicated for 15 min to obtain a homogeneous suspension. A stock suspension of 1 mg/mL rGO was prepared, and 100 µL of the suspension was introduced into each agar well (6 mm diameter). Sterile deionized water was used as the negative control, while standard antimicrobial agents were used as positive controls. For antibacterial assays, 100 µL of Ampicillin (1 mg/mL) was used against Gram-positive bacteria and 100 µL of Gentamicin (1 mg/mL) against Gram-negative bacteria. For antifungal assays, Amphotericin B (100 IU/disc) was employed as the reference antifungal agent. Following sample application, the plates were incubated at 37 °C for 24 h for bacterial cultures and at 28 °C for 48 h for fungal cultures. The antimicrobial activity was assessed by measuring the diameter of the inhibition zones in millimeters (mm). All experiments were performed in triplicate (n = 3), and the results were expressed as mean ± standard deviation (SD). Statistical analysis was carried out using one-way analysis of variance (ANOVA) followed by an appropriate post hoc test, and differences were considered statistically significant at $p < 0.05$.

*Assessment of cytotoxic effects using viability assay*

The VACSERA Tissue Culture Unit provided the mammalian colon (HCT-116) and breast (MCF-7) cancer cell lines. These lines were cultured under optimal growth conditions, i.e., maintained at 5% $CO_2$ atmosphere and 37 °C. Regular inspection of cells was performed using an inverted microscope. Using a cell counter and the 0.4% trypan blue exclusion test, the total number of cells for each trial was ascertained. Cells were plated in 96-well plates with 90 µl of optimized media at a density of $2 \times 10^5$ cells/well. Following a settling period of 24 hours, the cells were treated with eight different rGO nanosheet concentrations. After that, the treated cells were given another 24 hours to develop. Each experiment was conducted in quadruplicate. Values for optical density were normalized in relation to the untreated control cells. The cell viability numbers for untreated cells were therefore set at 100%, but the values for treated cells can be lower or higher than 100%. The following equation was used for calculations:

Cell viability (%) = ((Absorbance of the treated sample) / (Absorbance of the control)) X 100

## RESULTS AND DISCUSSION

*I. Characterization of rGO*

XRD plays a pivotal role in analyzing crystalline structure, identifying phases, and detecting lattice parameters of samples. Figure (2A) illustrates the XRD patterns of rGO synthesized via the green method utilizing NSS extract. The primary peak was observed at 25° (corresponding to (002) reflections and a d-spacing of approximately 0.35-0.36 nm). In the XRD spectrum, this wider and stronger peak center indicates the elimination of a substantial amount of the oxygen functional groups and is typical of reduced graphene oxide with few layers [16-18]. Likewise, Vinodhkumar, G. *et al.* [27], revealed that the XRD pattern of rGO has a broad diffraction peak at $2\theta$ = 18°-26°, which shows the partial restoration of carbon atoms in the graphite lattice and the gap between the graphene layers for oxygen and other functional groups. At $2\theta$ = 42.2°, a very small diffraction peak develops, probably as a result of incomplete oxidation. Accordingly, the XRD data indicate that NSS extract successfully reduced both epoxide and carboxyl functional groups, which is in line with earlier findings [19]. Table 1 summarizes the structural characteristics of the synthesized NSS-rGO nanosheets and compares them with those reported

for previously published graphene-based materials. The presence of the characteristic (002) diffraction peak confirms the successful reduction of graphene oxide and the restoration of the graphitic structure. The structural features of NS-rGO are comparable to those reported for other green- and chemically-reduced graphene oxide materials, demonstrating the effectiveness of the proposed synthesis approach.

Table 1. Comparison of the structural characteristics of the synthesized NS-rGO nanosheets with previously reported green- and chemically-synthesized graphene-based materials.

| Structural properties | | |
|---|---|---|
| Material/method | Main rGO peak (2θ, plane) & d-spacing | Structural note |
| NS-rGO (current work) | 25° (002), d = 0.1616 nm | Broad, strong (002) peak; few-layer rGO; substantial loss of oxygen groups |
| Chemically reduced HRG [20] | 23.4° (002), d ≈ 0.38–0.40 nm (graphite 26.5°, 0.34 nm; GO 13.4°, 0.66 nm) | Broad (002) peak; few-layer graphene, lower crystallinity than graphite |
| Chemically reduced rGO (various agents) [21] | rGO interlayer distance typically 0.4 nm vs GO ≈ 0.9 nm (6–7 layers → 2–3 layers) | Fewer layers and decreased d-spacing after reduction; C/O increased up to 10.3 |
| Green rGO (peptide–rGO, ascorbic acid) [22] | rGO shows a broad (002)-type peak; residual GO peak near 9° may persist (partial reduction) | Amorphous/exfoliated structure; incomplete removal of oxygen groups |
| Plasma-reduced rGO [23] | GO: 11.2° (001), d = 0.79 nm; rGO: 11.8°, d = 0.75 nm | Partial deoxygenation; d-spacing decreases but remains larger than graphite |
| Hydrazine-treated rGO (film, annealed) [24] | GO: d002 = 0.823 nm; HRGO300: d002 = 0.339 nm | Nearly graphitic spacing after strong reduction/annealing |

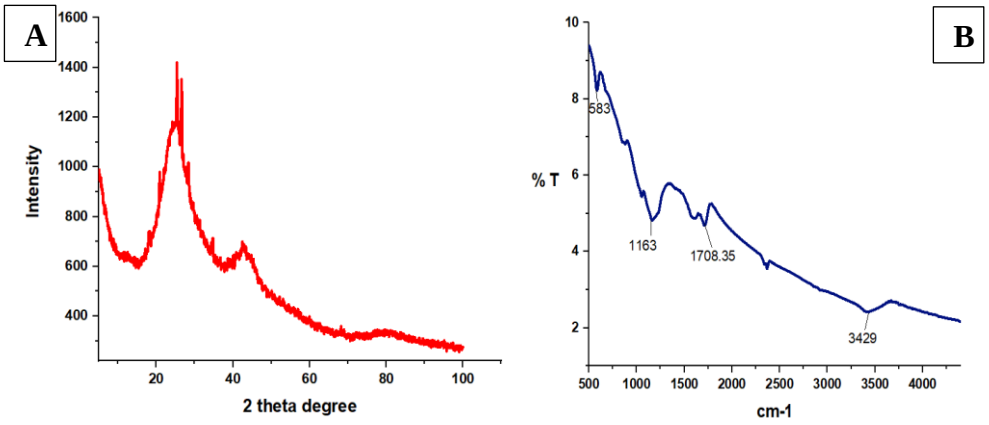


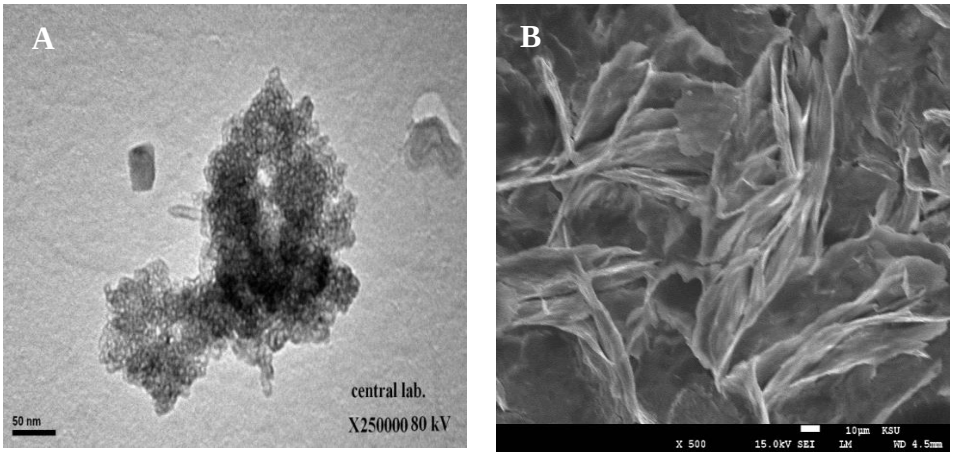

Figure 2. (A) X-ray diffraction patterns and (B) FTIR spectrum of green synthesized rGO.

The FTIR spectrum was used to further characterize the chemical structure of the prepared rGO nanosheets (Figure 2B). The overall spectrum exhibited a markedly low transmittance baseline, which, in the mid-infrared region, serves as a fundamental indication of the successful reduction process. Mujamammi, W.M. *et al.* [25] reported that pristine GO typically exhibits a higher transmittance baseline due to its highly oxidized, non-conductive, and

structurally disrupted nature. Consequently, the synthesized black rGO powder strongly absorbs and scatters incident infrared radiation, resulting in the characteristic flattened baseline observed in the spectrum. The broad and shallow absorption band centered at approximately 3429 $cm^{-1}$ is generally attributed to the stretching vibrations of hydroxyl (–OH) groups and intercalated water molecules trapped within the carbon layers. The weak peak observed at 1708.35 $cm^{-1}$ corresponds to the stretching vibration of carbonyl (C=O) groups associated with carbonyl and carboxylic acid functionalities. Botas *et al.* reported that because carboxyl groups are primarily located at the highly reactive, defective edges of graphene sheets, their complete removal generally requires high-temperature thermal treatment [26]. Therefore, the persistence of this weak band indicates a small amount of residual oxygen-containing defects, which is common in green-synthesized rGO materials. Furthermore, the distinct absorption peak at 1163 $cm^{-1}$ is assigned to the stretching vibrations of C–O bonds associated with alkoxy and epoxy groups, suggesting that a limited fraction of basal-plane oxygen bridges remains after the reduction process. The sharp band observed in the lower fingerprint region at approximately 583 $cm^{-1}$ is attributed to out-of-plane aromatic C–H bending vibrations or skeletal C–C lattice vibrations within the graphitic framework. The FTIR results confirm the substantial removal of oxygen-containing functional groups and support the successful reduction of graphene oxide while retaining a small amount of residual oxygen functionalities characteristic of green-synthesized rGO materials [27].

The resulting rGO's surface morphology was observed using TEM and SEM analyses, illustrated in Figures 3A and 3B, respectively. The TEM image (Figure 3A) illustrates that the single- or few-layer rGO nanosheets are highly transparent and exhibit some visible wrinkles and minor holes on the surface. Consistent with these results, the SEM analyses (Figure 3B) revealed that rGO nanosheets that appear less transparent display a significantly wrinkled and crumpled morphology. These findings suggest that the aggregation of graphene nanosheets during the reduction of graphene using NSS to create rGO results in the creation of a strongly pleated surface [28, 29, 16].

The elemental composition was estimated using EDS. The results (Figure 3C) reveal the presence of 98.85% carbon and 1.15% oxygen, indicating the high quality of the synthesized material [30, 16].



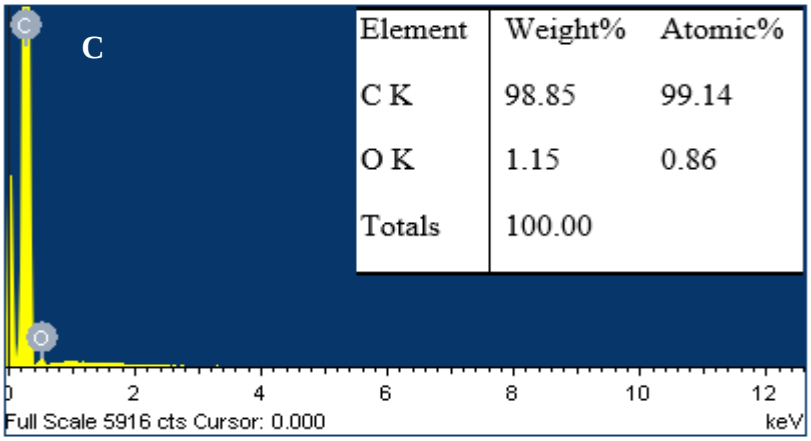



Figure 3. (A) TEM micrograph, (B) SEM image and (C) EDS spectrum of green synthesized rGO.

X-ray photoelectron spectroscopy (XPS) was employed to investigate the surface elemental composition and chemical states of the synthesized rGO nanosheets (Figure 4 (A and B)). The survey spectrum was dominated by the characteristic C 1s and O 1s signals, confirming carbon and oxygen as the major surface elements. The predominance of the carbon signal relative to oxygen is consistent with the formation of a carbon-rich structure following the oxidation and subsequent processing of the soot precursor. The O 1s region exhibited a broad asymmetric feature centered at approximately 531.5 eV (Figure 4A), reflecting the presence of different oxygen-containing chemical environments, including carbonyl, hydroxyl/epoxy, and other surface oxygen species [29-31]. To obtain further insight into the carbon bonding environments, the high-resolution C 1s spectrum was analyzed after charge correction by referencing the principal graphitic carbon component to 284.8 eV. The C 1s envelope was deconvoluted using a Shirley background and pseudo-Voigt line shapes, yielding three principal components centered at approximately 284.82, 286.01, and 288.91 eV. The dominant component at 284.82 eV accounted for approximately 61.1% of the total fitted C 1s area and was assigned primarily to C–C/C=C bonding associated with the graphitic carbon framework, indicating the presence of substantial $sp^2$-rich conjugated carbon domains. The component centered at 286.01 eV, representing approximately 26.8% of the fitted area, was attributed to C–O/C–O–C environments, whereas the higher-binding-energy component at 288.91 eV contributed approximately 12.1% and was associated with highly oxygenated carbon environments (Figure 4B). The predominance of the C–C/C=C component, together with the smaller contributions from oxygenated carbon species, indicates partial restoration of the conjugated graphitic network while confirming the persistence of oxygen-containing functional groups in the synthesized rGO. The C/O atomic ratio, calculated from the background-corrected integrated C 1s and O 1s peak areas using the appropriate sensitivity factors, was approximately 3.7, further supporting the carbon-rich nature and partial deoxygenation of the material. The residual oxygen-containing functionalities and structural defects may generate localized electronic states and interfacial polarization sites, providing a possible structural basis for the observed frequency-dependent dielectric and electrical behavior. Collectively, the XPS results support the formation of a partially reduced, structurally heterogeneous graphene-based carbon material containing restored graphitic domains together with residual oxygen functionalities, agreement with the FTIR and UV-Vis results.

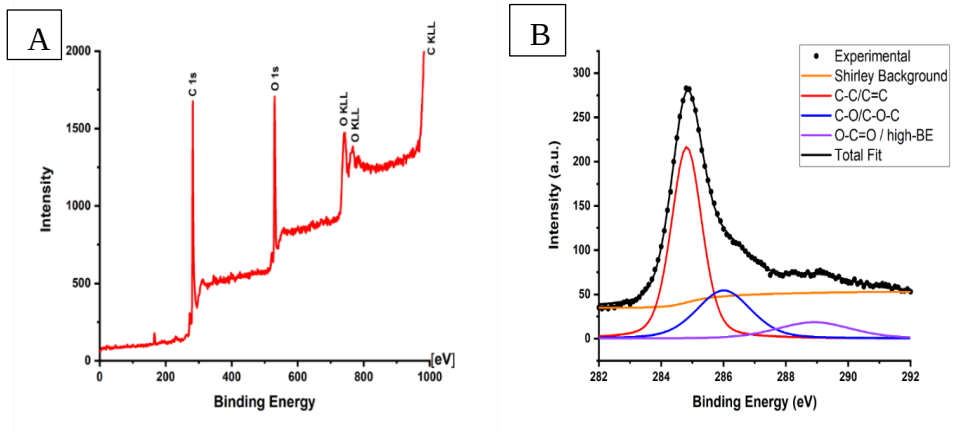



Figure 4. (A) XPS spectra and (B) high-resolution C 1s XPS spectrum and peak deconvolution of green-synthesized rGO.

The DLS analysis of NSS extract–rGO revealed a multimodal particle size distribution; the Z-average size of 385.2 nm and PDI of 0.441 confirm moderate polydispersity, as shown in Figure 5. The dominant nanosized fraction suggests effective exfoliation and reduction by NSS phytochemicals. The measured zeta potential of +17 ± 6.58 mV indicates moderate stability due to partial surface charge and residual functional groups [34]. Overall, NSS extract efficiently reduces and stabilizes rGO, though minor aggregation may occur due to limited electrostatic repulsion [35].

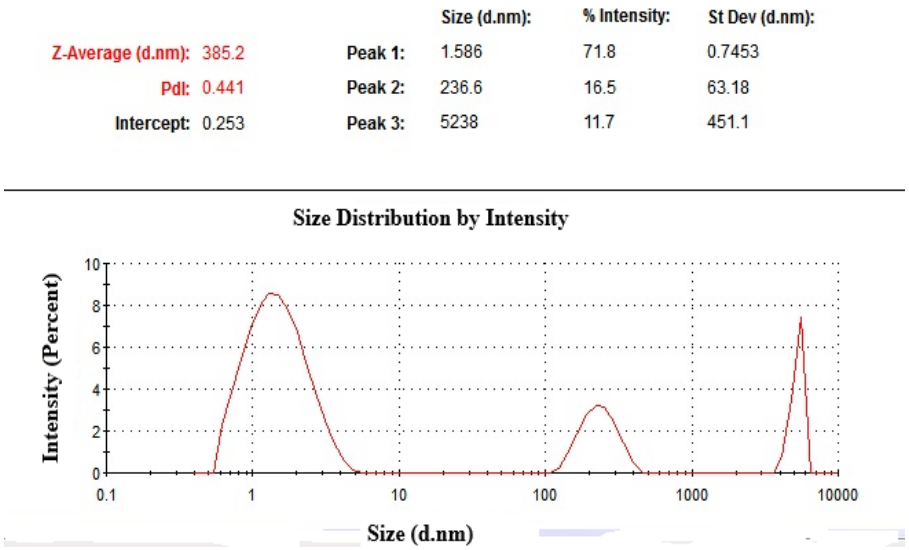



Figure 5. DLS measurements of the green-synthesized rGO.

*Antimicrobial and anticancer properties of rGO produced by reduction of graphene using NSS*

As indicated in Table 2, the antibacterial activity of rGO at different concentrations against Gram-positive, Gram-negative, and fungal pathogens was evaluated using the agar well diffusion method. The results demonstrated that the synthesized rGO exhibited considerable antimicrobial activity against most of the tested microorganisms, with the highest inhibition observed against *Bacillus subtilis*, followed by *Aspergillus fumigatus, Streptococcus pneumoniae*, *Escherichia coli, Candida albicans, and Pseudomonas aeruginosa*. Furthermore, the observed inhibition zones indicate promising antimicrobial activity of the synthesized rGO under the tested conditions, while the standard antibiotics served as reference controls. The antimicrobial mechanism of rGO is believed to involve multiple pathways (Figure 6), including direct physical disruption of microbial cell membranes by the sharp edges of graphene sheets, adsorption and isolation of microbial cells from their surrounding environment, and the induction of oxidative stress through the generation of reactive oxygen species (ROS). These effects can compromise membrane integrity, disrupt cellular metabolism, and ultimately lead to cell death. In addition, residual oxygen-containing functional groups on the rGO surface may enhance interactions with microbial cell walls, contributing to its antimicrobial performance [33, 36]. Although the present results demonstrate promising antimicrobial activity, further investigations regarding biocompatibility, toxicity, and in vivo performance are required before practical biomedical applications can be established.

Table 2. Antimicrobial activity of NSS- rGO against various fungal and bacterial strains.

| Microorganisms | rGO | St. |
|---|---|---|
| Fungi | *Amphotericin B* | |
| *Aspergillus fumigatus* (RCMB 02567) | 33.3 ± 1.5 | 21.7 ± 1.5 |
| *Candida albicans* (RCMB 05038) | 19.3 ± 1.5 | 22.7 ± 1.5 |
| Gram-positive bacteria: | *Ampicillin* | |
| *Streptococcus pneumoniae* (RCMB 010011) | 32.7 ± 2.1 | 21.0 ± 1.0 |
| *Bacillus subtilis* (RCMB 010068) | 34.0 ± 2.0 | 31.3 ± 1.5 |
| Gram-negative bacteria: | *Gentamicin* | |
| *Pseudomonas aeruginosa* (RCMB 010045) | 16.3 ± 2.1 | 16.0 ± 1.0 |
| *Escherichia coli* (RCMB 010054) | 26.3 ± 2.1 | 20.3 ± 0.58 |




Figure 6. Diagram of possible mechanisms of biomedical activities of rGO.

rGO demonstrated significant dose-dependent cytotoxicity against colon and breast cancer cells. Cell viability, dependent on mitochondrial activity, was quantified using the MTT assay. For 24 hours, the cells were exposed to rGO at progressively higher concentrations. For MCF-7 and HCT-116 cell lines, the half-maximal inhibitory concentration ($IC_{50}$) of rGO was determined to be 3.125 mg/mL and 1.56 mg/mL, respectively (Figure 7(A and B)).

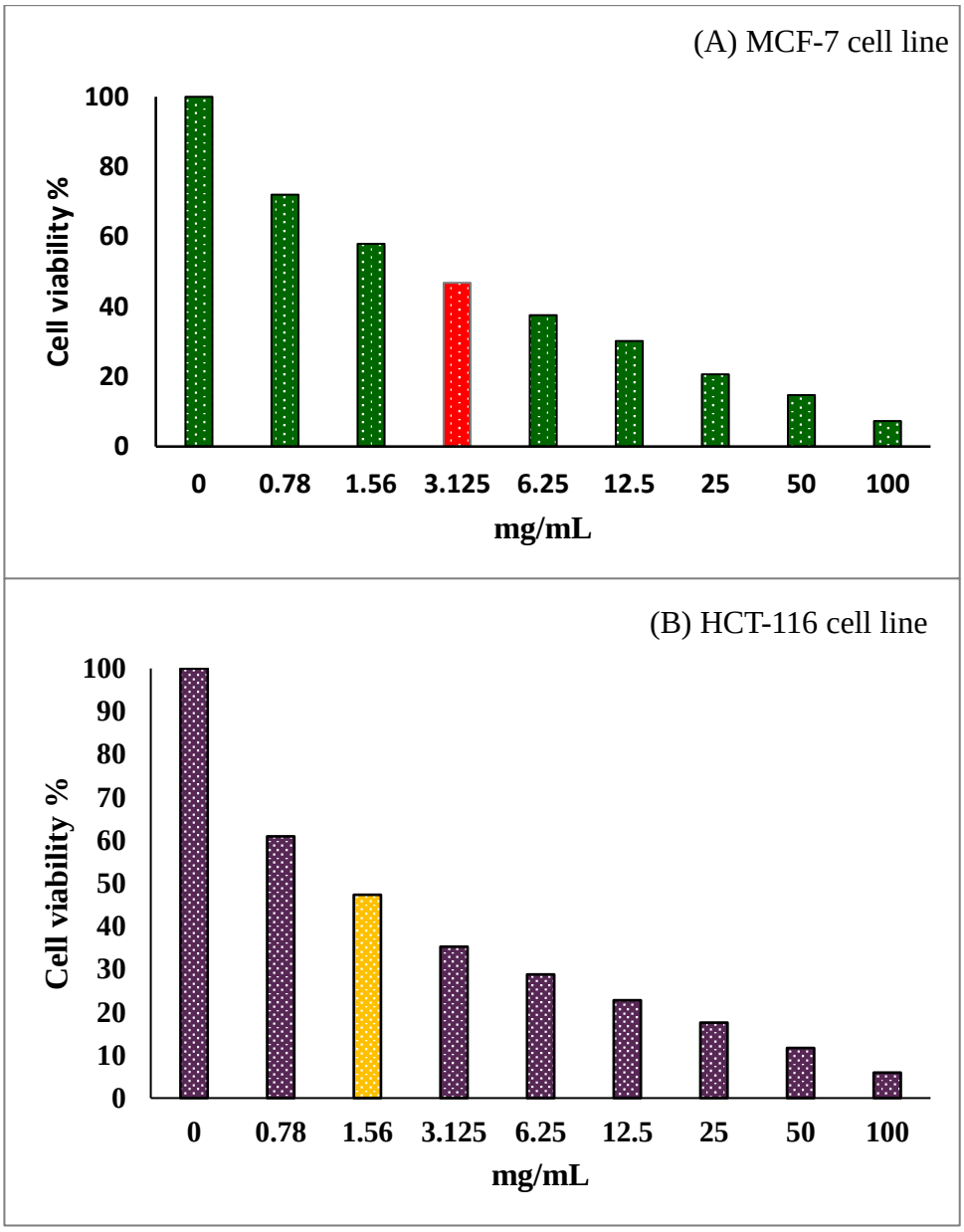



Figure 7. Cytotoxic activity of NSS-rGO against (A) MCF-7 and (B) HCT-116 cell lines.

Previous studies have demonstrated that rGO sheets can effectively accumulate on the surface of cancer cells and facilitate intracellular transport, thereby enhancing their biological activity [37-39]. Once internalized, rGO nanosheets may induce the generation of reactive oxygen species (ROS), leading to oxidative stress and subsequent damage to essential cellular biomolecules such as DNA, proteins, and lipids (Figure 6). This oxidative imbalance can trigger multiple cell death pathways, including apoptosis and necrosis, ultimately inhibiting cancer cell proliferation. Furthermore, rGO has been reported to stimulate autophagy, a cellular self-degradation process that can contribute to cancer cell death under excessive stress conditions [30-42]. The observed cytotoxic effects are consistent with previous findings, including those reported by Gurunathan *et al.*, who demonstrated the anticancer potential of resveratrol-reduced rGO against human lung cancer cells [43]. These findings highlight the promising therapeutic potential of green-synthesized rGO nanosheets as anticancer agents. However, the present study evaluated cytotoxicity only against cancer cell lines, and no assessment was performed using normal (non-cancerous) mammalian cells. Therefore, comprehensive biocompatibility and selectivity assessments using appropriate normal mammalian cell lines are essential and should be undertaken in future studies to establish the safety profile, selectivity index, and therapeutic window of the synthesized nanomaterial, thereby facilitating its potential biomedical translation [44, 45]. Table 3 presents a comparison of the antimicrobial and anticancer properties of the synthesized NS-rGO nanosheets and previously reported graphene-based materials prepared using green and chemical reduction methods.

Table 3. Comparative analysis of the biomaedical properties of the synthesized NS-rGO nanosheets with those of previously reported graphene-based nanomaterials.

| Biological properties | | |
|---|---|---|
| Material/method | Antibacterial profile | Anticancer/cytotoxicity ($IC_{50}$, exposure) |
| NS-rGO (current work) | Strong, broad-spectrum; highest vs *B. subtilis*, then *A. fumigatus*, *S. pneumoniae*, *E. coli*, *C. albicans*, *P. aeruginosa*; zones greater than standard | MCF-7 $IC_{50}$= 3.125 mg/mL; HCT-116 $IC_{50}$ = 1.56 mg/mL (24 h, MTT) |
| Green tea rGO [46] | Strong vs *E. coli*, *Staphylococcus*; notable antioxidant activity | High toxicity to MCF-7 and PC3; $IC_{50}$ not numerically specified |
| Chenopodium-rGO [47] | Enhanced vs Gram+ and Gram– vs GO; antibiofilm improved | MCF-7 viability drops from 90%→35% between 1-250 µg/mL (dose-dependent) |
| Acalypha / Raphanus-rGO [48] | Not reported | A549 $IC_{50} \approx$ 26.7-38.5 µg/mL; MCF-7 $IC_{50} \approx$ 33-36 µg/mL |
| Euphorbia-rGO [49] | Not reported | Significant cytotoxicity vs A549, HepG2 (values not specified) |
| Chemically reduced HRG [20] | Strong vs Gram+ (*B. subtilis*, MRSA, *S. aureus*), similar to ampicillin; high antibiofilm activity | MCF-7 $IC_{50} \approx$ 29.5 µg/mL |
| N-doped graphene (hydrazine) [50] | Better vs Gram+ (MRSA, *B. subtilis*, *S. pneumoniae*, *S. mutans*); no activity vs *K. pneumoniae*, *P. aeruginosa* | MCF-7 $IC_{50}$ 27.15 µg/mL; HeLa 30.85 µg/mL |

## CONCLUSION

In conclusion, this study demonstrated a green and environmentally friendly approach for the synthesis of reduced graphene oxide rGO nanosheets using Nigella sativa seed (NSS) extract as a natural reducing agent. Structural, morphological, and surface characterization analyses, including XRD, EDX, SEM, TEM, FTIR, and XPS, confirmed the successful synthesis of rGO nanosheets. The XRD results revealed the characteristic graphitic structure of rGO, while EDX analysis confirmed the predominance of carbon in the synthesized material. Furthermore, SEM and TEM observations demonstrated the formation of crumpled and wrinkled nanosheets, which are characteristic features of rGO. The synthesized NSS-rGO nanosheets exhibited promising in vitro antibacterial and antifungal activities against various microbial strains, as well as significant cytotoxic effects against MCF-7 and HCT-116 cancer cell lines. These findings highlight the potential of green-synthesized rGO nanosheets for future biomedical applications. However, further investigations, including comprehensive biocompatibility and toxicity assessments using normal cell lines, mechanistic studies, long-term stability evaluations, and in vivo validation, are required before their biomedical and therapeutic potential can be fully established.

## ACKNOWLEDGEMENTS

The authors acknowledge the Research Institute /Centre supporting program (ORF-RICSP-2026-2BT), King Saud University, Riyadh, Saudi Arabia.

*Data availability*

All data are available upon request.

*Conflicts of interest*

The authors declare no conflict of interest.

*Author statement*

Conceptualization, Manal Awad and Khalid Ortashi; Data curation, Khalid Ortashi; Formal analysis, Khalid Ortashi and Manal Awad; Investigation, Manal Awad; Methodology, Manal Awad, H. Alrsheed, Wadha Alenazi; Resources, Manal Awad and Khalid Ortashi; Software, Mervat Alamri; Validation, Manal Awad; Writing – original draft, Manal Awad, Eram Eltahir, Fatemah M. Barakat and Khalid Ortashi; Writing – review & editing Manal Awad.

## REFERENCES

1. Worku, A.K.; Ayele, D.W. Recent advances of graphene-based materials for emerging technologies. *Results Chem*. **2023**, 5, 100971-100985.
2. Narayan, J.; Bezborah, K. Recent advances in the functionalization, substitutional doping and applications of graphene/graphene composite nanomaterials. *RSC Adv*. **2024**, 14, 13413-13444.
3. Tyson, J.A.; Calatayud, D.G.; Mirabello, V.; Mao, B.; Pascu, S.I. Labeling of graphene, graphene oxides, and their congeners: Imaging and biosensing applications relevant to cancer theranostics. *Adv. Inorg. Chem*. **2016**, 68, 397-440.
4. Mekassa, B.; Baker, P. G.; Chandravanshi, B. S.; Tessema, M. Sensitive electrochemical determination of ethambutol in pharmaceutical formulation and human urine at nickel

nanoparticles/electrochemically reduced graphene oxide modified electrode. *Bull. Chem. Soc. Ethiop*. **2019**, 33, 215-228.
5. Sanmugam, A.; Abbishek, S.; Kumar, S.L.; Sairam, A.B.; Palem, V.V.; Kumar, R.S.; Vikraman, D. Synthesis of chitosan-based reduced graphene oxide–$CeO_2$ nanocomposites for drug delivery and antibacterial applications. *J. Mech. Behav. Biomed. Mater*. **2023**, 145, 106033-106043.
6. Qin, C.; Fei, J.; Cai, P.; Zhao, J.; Li, J. Biomimetic membrane-conjugated graphene nanoarchitecture for light-manipulating combined cancer treatment in vitro. *J. Colloid Interface Sci*. **2016**, 482, 121-130.
7. Dasari Shareena, T.P.; McShan, D.; Dasmahapatra, A.K.; Tchounwou, P.B. A review on graphene-based nanomaterials in biomedical applications and environmental and health risks. *Nano-Micro Lett*. **2018**, 10, 1-34.
8. Patil, S.; Rajkuberan, C.; Sagadevan, S. Recent biomedical advancements in graphene oxide and future perspectives. *J. Drug Deliv. Sci. Technol*. **2023**, 81, 104737-104753.
9. Adekoya, O. C.; Adekoya, G. J.; Kupolati, W. K.; Hamam, Y.; Sadiku, R. E. Polyethylene glycol-functionalized graphene oxide nanocomposites: Advances in biomedical applications. *Nano Select*. **2025**, 6, e70051-e70090.
10. Moghadam, N.B.; Avatefi, M.; Karimi, M.; Mahmoudifard, M. Graphene family in cancer therapy: Recent progress in cancer gene/drug delivery applications. *J. Mater. Chem. B.* **2023**, 11, 2568-2613.
11. Ma, J.; Liu, C.; Li, R.; Wang, J. Properties and structural characterization of oxide starch/chitosan/graphene oxide biodegradable nanocomposites. *J. Appl. Polym. Sci.* **2012**, 123, 2933-2944.
12. Feng, L.; Liu, Z. Graphene in biomedicine: Opportunities and challenges. *Nanomedicine* **2011**, 6, 317-324.
13. Deepa, C.; Rajeshkumar, L.; Ramesh, M. Preparation, synthesis, properties and characterization of graphene-based 2D nanomaterials for biosensors and bioelectronics. *J. Mater. Res. Technol*. **2022**, 19, 2657-2694.
14. Ge, Z.; Yang, L.; Xiao, F.; Wu, Y.; Yu, T.; Chen, J.; Zhang, Y. Graphene family nanomaterials: Properties and potential applications in dentistry. *Int. J. Biomater*. **2018**, 2018, 1539678-1539690.
15. Awad, M.A.; Hendi, A.A.; Ortashi, K.M.O.; Laref, A. Green synthesis of reduced graphene oxide using Nigella sativa seed extract. US Patent 9688539 B1, **2017**.
16. Perveen, F.; Ullah, F.; Rehman, A.; Zaman, H.; Abbas, W.; Khan, M.; Bilal, M.; Khan, A.; Ullah, L. A. Review on nanotechnology-driven green synthesis of silver nanoparticles using Nigella sativa. *Insights J. Health Rehabil*. **2025**, 3, 121-28.
17. Liu, Y.Y.; Luo, S.H.; Yan, S.X.; Feng, J.; Yi, T.F. Green synthesis of reduced graphene oxide as high-performance electrode materials for supercapacitors. *Ionics* **2020**, 26, 415-422.
18. Eluyemi, M.S.; Eleruja, M.A.; Adedeji, A.V.; Olofinjana, B.; Fasakin, O.; Akinwunmi, O.O.; Ajayi, E.O.B. Synthesis and characterization of graphene oxide and reduced graphene oxide thin films deposited by spray pyrolysis. *Graphene* **2016**, 5, 143-154.
19. Coros, M.; Pogacean, F.; Turza, A.; Dan, M.; Berghian-Grosan, C.; Pana, I.O.; Pruneanu, S. Green synthesis, characterization and potential application of reduced graphene oxide. Physica E Low-Dimens. *Syst. Nanostruct*. **2020**, 119, 113971-113979.
20. Alangari, A.; Mateen, A.; Alqahtani, M.; Shahid, M.; Syed, R.; Shaik, M.; Khan, M.; Adil, S.; Kuniyil, M. Antimicrobial, anticancer, and biofilm inhibition studies of highly reduced graphene oxide (HRG): In vitro and in silico analysis. *Front. Bioeng. Biotechnol.* **2023**, 11, 1149588-1149600.
21. Lesiak, B.; Trykowski, G.; Tóth, J.; Biniak, S.; Kövér, L.; Rangam, N.; Stobiński, L.; Małolepszy, A. Chemical and structural properties of reduced graphene oxide—dependence on the reducing agent. *J. Mater. Sci.* **2020,** 56, 3738-3754.

22. Joshi, S.; Siddiqui, R.; Sharma, P.; Kumar, R.; Verma, G.; Saini, A. Green synthesis of peptide functionalized reduced graphene oxide (rGO) nano bioconjugate with enhanced antibacterial activity. *Sci. Rep*. **2020**,10, 9441-9452.
23. Hazarika, T.; Ghosh, R.; Saikia, G.; Kakati, B.; Rajbongshi, T.; Das, M.; Kundu, S.; Biswas, S.; Kalita, H. Controlled reduction of graphene oxide (GO) film using low-density glow discharge hydrogen plasma. *IEEE Trans. Plasma Sci*. **2025**, 53, 1025-1036.
24. Ochigbo, S.; Obar, A.; Suleiman, M.; Kovo, A. Facile synthesis and optimization of graphene oxide reduction by annealing in hydrazine vapour in ambient air for potential application in perovskite solar cells. *Sci. World J*. **2024,** 19, 194-199.
25. Mujamammi, W.M.; Aldbas, H.A.; AlShehri, H. A.; Awad, M.A. Graphite, graphene oxide, and reduced graphene oxide: Comparative characterization of optical, morphological, structural and electric relaxation properties. *Green Process. Synth*. **2026,** 15, 20250113-20250123.
26. Botas, C.; Álvarez, P.; Blanco, C.; Santamaría, R.; Granda, M.; Gutiérrez, M. D.; Menéndez, R. Critical temperatures in the synthesis of graphene-like materials by thermal exfoliation–reduction of graphite oxide. *Carbon* **2013**, 52, 476-485.
27. Vinodhkumar, G.; Ramya, R.; Vimalan, M.; Potheher, I.; Cyrac Peter, A. Reduced graphene oxide for simultaneous detection of neurotransmitters. *Prog. Chem. Biochem. Res.* **2018**, 1, 1-59.
28. Almatroudi, A.; Khadri, H.; Azam, M.; Rahmani, A.H.; Al Khaleefah, F.K.; Khateef, R.; Allemailem, K.S. Antibacterial, antibiofilm and anticancer activity of biologically synthesized silver nanoparticles using *Nigella sativa* seed extract. *Processes* **2020**, 8, 388-402.
29. Hulagabali, M.M.; Vesmawala, G.R.; Patil, Y.D. Synthesis, characterization, and application of graphene oxide and reduced graphene oxide and its influence on rheology, microstructure, and mechanical strength of cement paste. *J. Build. Eng*. **2023**, 71, 106586- 106607.
30. Sinha, A.; So, H. Structural effects of crumpled graphene and recent developments in comprehensive sensor applications: A review. *Small Struct*. **2023**, 4, 2300084-2300105.
31. Kumuda, S.; Gandhi, U.; Mangalanathan, U.; Rajanna, K. Synthesis and characterization of graphene oxide and reduced graphene oxide chemically reduced at different time durations. *J. Mater. Sci.: Mater. Electron*. **2024**, 35, 637-952.
32. Capezza, A.; Andersson, R.L.; Ström, V.; Wu, Q.; Sacchi, B.; Farris, S.; Olsson, R.T. Preparation and comparison of reduced graphene oxide and carbon nanotubes as fillers in conductive natural rubber for flexible electronics. *ACS Omega*. **2019**, 4, 3458-3468.
33. Bagri, A.; Mattevi, C.; Acik, M.; Chabal, Y.J.; Chhowalla, M.; Shenoy, V.B. Structural evolution during the reduction of chemically derived graphene oxide. *Nat. Chem*. **2010**, 2, 581-588.
34. Estrade-Szwarckopf, H. XPS photoemission in carbonaceous materials: A "defect" peak beside the graphitic asymmetric peak. *Carbon.* **2004**, 42, 1713-1721.
35. Koinuma, M.; Tateishi, H.; Hatakeyama, K.; Miyamoto, S.; Ogata, C.; Funatsu, A.; Matsumoto, Y. Analysis of reduced graphene oxides by X-ray photoelectron spectroscopy and electrochemical capacitance. *Chem. Lett*. **2013**, 42, 924-926.
36. Saini, R.; Mishra, R.K.; Kumar, P. Green synthesis of reduced graphene oxide using *Tinospora cordifolia* plant extract: Exploring its potential for methylene blue dye degradation and antibacterial activity. *ACS Omega* **2024**, 9, 20304-20321.
37. Ahamed, M.; Akhtar, M.J.; Khan, M.M.; Alhadlaq, H.A. A novel green preparation of Ag/RGO nanocomposites with highly effective anticancer performance. *Polymers* **2021**, 13, 3350-3364.
38. Abdullah, M.F.; Zakaria, R.; Zein, S.H.S. Green tea polyphenol–reduced graphene oxide: Derivatisation, reduction efficiency, reduction mechanism and cytotoxicity. *RSC Adv*. **2014**, 4, 34510-34518.

39. Thiyagarajulu, N.; Deepak, P.; Kamaraj, C.; Al-Ghanim, K.A.; Lakshminarayanan, A.; Nicoletti, M.; Govindarajan, M. Synthesis and characterization of reduced graphene oxide nanosheets using *Saraca indica* leaves and their antioxidant, antibacterial, and anticancer applications. *Biomass Convers. Biorefin*. **2023**, 14, 1-15.
40. AbouAitah, K.; Sabbagh, F.; Kim, B.S. Graphene oxide nanostructures as nanoplatforms for delivering natural therapeutic agents: Applications in cancer treatment, bacterial infections, and bone regeneration medicine. *Nanomaterials* **2023**, 13, 2666-2704.
41. Sharma, H.; Mondal, S. Functionalized graphene oxide for chemotherapeutic drug delivery and cancer treatment: A promising material in nanomedicine. *Int. J. Mol. Sci.* **2020**, 21, 6280-6322.
42. Zhang, J.; Cao, H.Y.; Wang, J.Q.; Wu, G.D.; Wang, L. Graphene oxide and reduced graphene oxide exhibit cardiotoxicity through the regulation of lipid peroxidation, oxidative stress, and mitochondrial dysfunction. *Front. Cell Dev. Biol*. **2021**, 9, 616888-616898.
43. Gurunathan, S.; Han, J.; Kim, E. S.; Park, J.; Kim, J. Reduction of graphene oxide by resveratrol: A novel and simple biological method for the synthesis of an effective anticancer nanotherapeutic molecule. *Int. J. Nanomed*. **2015**, 10, 2951-2969.
44. Awad, M. A.; Ortashi, K. M.; Alabodi, N.; Hagmusa, A.; Hagmusa, B. A facile synthesis of crystalline eggshell nanostructures: Characterization and assessment of their potential for biomedical applications. *Bull. Chem. Soc. Ethiop*. **2026,** 40, 383-394.
45. Bhatt, S.; Pathak, R.; Punetha, V.D.; Punetha, M. Recent advances and mechanism of antimicrobial efficacy of graphene-based materials: A review. *J. Mater. Sci.* **2023**, 58, 7839-7867.
46. Vatandost, E.; Saraei, A.; Chekin, F.; Raeisi, S.; Shahidi, S. Antioxidant, antibacterial and anticancer performance of reduced graphene oxide prepared via green tea extract assisted biosynthesis. *ChemistrySelect* **2020**, 5, 10401-10406.
47. Umar, M.; Ahmad, F.; Saeed, H.; Usmani, S.; Owais, M.; Rafatullah, M. Bio-mediated synthesis of reduced graphene oxide nanoparticles from chenopodium album: Their antimicrobial and anticancer activities. *Nanomaterials* **2020**, 10, 1096-1109.
48. Punniyakotti, P.; Aruliah, R.; Angaiah, S. Facile synthesis of reduced graphene oxide using *Acalypha indica* and *Raphanus sativus* extracts and their in vitro cytotoxicity activity against human breast (MCF-7) and lung (A549) cancer cell lines. *3 Biotech*. **2021**, 11, 157-168.
49. Lingaraju, K.; Naika, R.; Nagaraju, G.; Nagabhushana, H. Biocompatible synthesis of reduced graphene oxide from *Euphorbia heterophylla* (L.) and their in-vitro cytotoxicity against human cancer cell lines. *Biotechnol. Rep*. **2019**, 24, e00376- e00384.
50. Alangari, A.; Aldakheel, F.; Mateen, A., Alqhatani, M.; Alaofi, A.; Shahid, M.; Ali, R.; Syed, R.; Adil, S.; Khan, M.; Kuniyil, M.; Shaik, M. Assessment of physicochemical, anticancer, antimicrobial, and biofilm activities of n-doped graphene. *Crystals* **2022**, 12, 1035-1048.